
QuEST: Low-bit Diffusion Model Quantization via Efficient Selective Finetuning

Haoxuan Wang¹ Yuzhang Shang¹ Zhihang Yuan² Junyi Wu¹ Junchi Yan³ Yan Yan¹
¹ Illinois Institute of Technology ² Infini AI ³ Shanghai Jiao Tong University
hwang220@hawk.iit.edu

Abstract

The practical deployment of diffusion models still suffers from the high memory and time overhead. While quantization paves a way for compression and acceleration, existing methods unfortunately fail when the models are quantized to low-bits. In this paper, we empirically unravel three properties in quantized diffusion models that compromise the efficacy of current methods: imbalanced activation distributions, imprecise temporal information, and vulnerability to perturbations of specific modules. To alleviate the intensified low-bit quantization difficulty stemming from the distribution imbalance, we propose finetuning the quantized model to better adapt to the activation distribution. Building on this idea, we identify two critical types of quantized layers: those holding vital temporal information and those sensitive to reduced bit-width, and finetune them to mitigate performance degradation with efficiency. We empirically verify that our approach modifies the activation distribution and provides meaningful temporal information, facilitating easier and more accurate quantization. Our method is evaluated over three high-resolution image generation tasks and achieves state-of-the-art performance under various bit-width settings, as well as being the first method to generate readable images on full 4-bit (i.e. W4A4) Stable Diffusion. Code is available [here](#).

1 Introduction

Diffusion models [6, 15, 32] have achieved great success in the field of image generation recently. Given the high capacity and flexibility of diffusion models, there still remains two challenges that limit their efficiency [4]. The first obstacle is the time-consuming denoising process which requires hundreds to thousands of inference time steps that slows down the generation speed drastically. The other one is the increasing model size driven by the need of better image fidelity and higher image resolutions. Both factors contribute to considerable latency and increased computational requirements, impeding the application of diffusion models to real-world settings where both time and computational power are carefully restricted.

Neural network quantization offers a feasible solution for accelerating inference speed and reducing memory consumption simultaneously [9]. It aims to compress high-bit model parameters into low-bit approximations with negligible performance degradation. For example, 4-bit weight and 4-bit activation quantization can achieve up to $8\times$ inference time speedup and $8\times$ memory reduction theoretically [23]. The benefits will increase consistently when the bit-widths are further lowered. Hence, low-bit quantization of diffusion models emerges as a viable approach for efficiency enhancement.

However, existing diffusion model quantization approaches fail under low-bit settings. These methods focus either on timestep-aware calibration data construction [19, 34] or quantization noise correction [12], targeting at tailoring existing quantization techniques to the properties of diffusion models that are distinct from other model types such as CNNs [31] and ViTs [2]. Such approaches overlook the intrinsic diffusion model mechanisms that are related with quantization, leading to inconsistencies

between method deployment and model characteristics. Therefore, we intend to identify unique features in diffusion models that are associated with quantization.

In this paper, we reveal three properties of quantized diffusion models that hinder effective quantization: ❶ The activation distributions are likely to be imbalanced, where the majority of values are close to 0 but the important and large values are rare and appear inconsistently. Conventional quantization methods tend to either approximate the large and sparse values, inadequately estimating the numerous small values, or focus on small values while overlooking the large ones, thereby impeding the reduction of quantization error. ❷ Diffusion models exhibit varying functions at distinct time steps [3], such as forming object outlines at early time steps and constructing details latter. Thus, preserving accurate temporal information is important during quantization. However, current methods struggle to represent extensive time steps with limited bit-width, leading to similar time embeddings across different time steps and results in error accumulation. ❸ Diffusion models typically have complex network architectures, incorporating convolutional layers and linear layers that construct various kinds of attention blocks [7] and residual blocks [10]. Whereas previous works consider each model component as equally important and apply quantization uniformly, we reveal that certain layers are particularly sensitive to perturbations from quantization, while others are more resilient.

Addressing the revealed properties, we propose a novel quantization approach for diffusion models, termed QuEST (Quantization via Efficient Selective FineTuning). Confronting property ❶, we first theoretically justify that weight fine-

tuning can enhance model robustness towards large perturbations in activations under low-bit settings for reducing quantization error, whereas previous methods struggle to find appropriate quantization parameters. Then we empirically show that by finetuning the model, the activation distributions are actually modified to be more amenable to quantization by reducing the significant values (large yet sparse), as shown in Figure 1(a). Following the idea of weight finetuning, we compare different bit-width models (Figure 1(b)) and identify two types of layers that are responsible for performance degradation: Time embedding layers exhibiting property ❷ and attention-related layers corresponding to property ❸. Thus, we selectively and progressively finetune these small layer subsets in conjunction with all activation quantization parameters, as illustrated in Figure 1(c). With less than 10% of the total parameters involved, QuEST not only substantially enhances low-bit quantized model performance, but is also notably time-efficient and requires only supervision from the full-precision model in a data-free manner. Our contributions are summarized as follows:

- We uncover and validate three properties that present challenges to low-bit diffusion model quantization: imbalanced activation distributions, imprecise temporal information, and vulnerability to perturbations of specific modules. We also theoretically discuss why previous methods are expected to fail and justify the sufficiency of weight finetuning under low-bit settings.
- Addressing the identified properties, we introduce QuEST, a new finetuning strategy that trains the model selectively and progressively, achieving low-bit quantization capability with high time and memory efficiency. An efficient activation quantizer is also proposed for time information estimation. Our method can be executed in a data-free and parameter-efficient manner.
- Experiments on three high-resolution image generation tasks over four models demonstrate the superiority of our method, achieving state-of-the-art performance under various bit-width settings. We are also the first method to generate reasonable images for full 4-bit Stable Diffusion.

The detailed related works on diffusion model inference and quantization are referred to appendix for space restriction. Table 1 is a compact summary that shows the unique capabilities of our method, where we are able to overcome the limitations of previous quantization methods. **In comparison with EfficientDM [11]**, we include a brief discussion here: Technically, EfficientDM aims to finetune via low-rank weight representations [16]. However, it introduces additional parameters for each layer and requires extensive iterations of training on LoRA weights. Our method instead does not include additional parameters and only needs to finetune the model for limited iterations with the same batch size. We have also found that EfficientDM does not quantize the matrix multiplications in the attention mechanism, while we quantize the matrices to 8-bits. Moreover, EfficientDM always keeps the first three layers and the last layer as full 8-bit (weight and activation), as well as keeping skip-connections and some linear layers as full-precision during implementation. Our method instead only kept the first and last layer as 8-bit and quantize all other layers to the required bit-width.

Table 1: Comparison with different frameworks.

METHOD	DATA FREE	TIME & MEMORY EFFICIENT	LOW-BIT COMPATIBLE	FULLY QUANTIZED
PTQ [19]	✓	✓	✗	✓
QAT [20]	✗	✗	✓	✓
EFFICIENTDM [11]	✓	✓	✓	✗
OURS	✓	✓	✓	✓

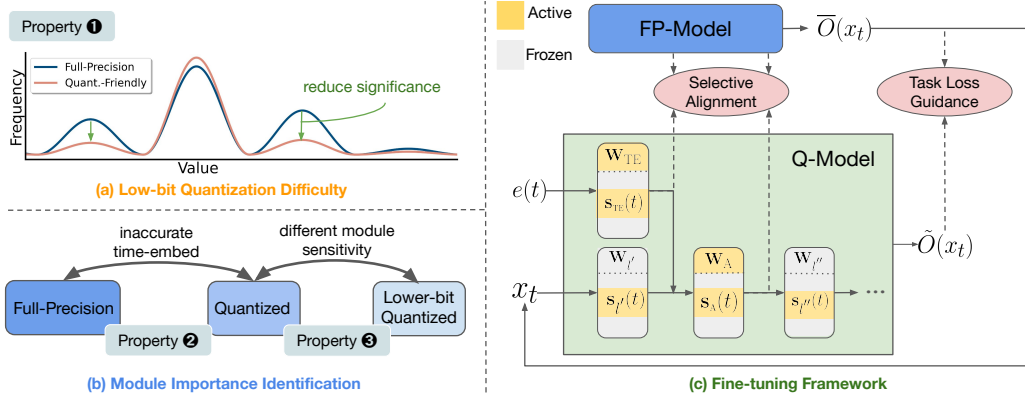


Figure 1: Overview of our findings and method. (a) Illustration of property ❶ and a way to mitigate the quantization difficulty. (b) Demonstration of how property ❷ and property ❸ are identified via comparing different bit-width models. (c) Framework of the proposed method at time step t . To address the quantization difficulty and achieve more quantization-friendly activation distribution efficiently, we **reduce significance** by selectively and progressively updating partial model layers’ weights. $e(t)$ and x_t are the input time embedding and input image representation respectively. While W_{TE} and W_A are selected layer weights to be optimized using Equation 8, $W_{l'}$ and $W_{l''}$ are frozen during finetuning. More details are included in Section 2.3.2.

2 Methodology

2.1 Preliminaries

The quantization process for a single value x in a vector can be formulated as:

$$\hat{x} = \text{clamp}(\text{round}(\frac{x}{s}) + Z; q_{min}, q_{max}), \quad (1)$$

where \hat{x} is the quantized integer result, $\text{round}(\cdot)$ represents rounding algorithms such as the round-to-nearest operator [22] and AdaRound [27], s is referred to as the scaling factor and Z is the zero-point. clamp is the function that clamps values into the range of $[q_{min}, q_{max}]$, which is determined by the bit-width. Reversely, transforming the quantized values back into the full-precision form is:

$$\tilde{x} = (\hat{x} - Z) * s. \quad (2)$$

This is denoted as the dequantization process. The quantization and dequantization processes are performed on both model weights and layer outputs (also termed as ‘activation’). Equation 1 indicates that the quantization error is composed of two factors: The clipping error produced by range clamping and the rounding error caused by the rounding function, where they exhibit a trade-off relationship [22]. While previous approaches strive for an optimal balance between the two errors, they neglect the intrinsic mechanisms in quantized diffusion models. In the next section, we investigate three properties of diffusion models that relate to quantization performance and show why typical quantization methods tend to fail.

2.2 Quantization-aware Properties of Diffusion Models

Property ❶: *The activation outputs are likely to have a majority of values close to zero, with the other values being numerically large and important.* Previous works [19, 34] paid attention to the varying activation distribution over different time steps, but none of them focused on the activation distribution itself. In Figure 2, we cluster activation values into uniformly distributed bins and manipulate the frequency for better visualization. We find that in some layers, though the majority of values are close to 0, there exists values that are relatively large and diverse, which we term as “significant values” (circled in green). Take the bin plot on the left for example, the original activation values (blue line) ranges from $[-10, 34]$ but with over 99% values between $[-0.6, 1.7]$. More visualizations can be found in Figure 6. This phenomenon poses difficulties in minimizing the clipping error and is unfriendly for effective quantization.

Moreover, we observe that these significant values are important for generation performance preservation (see Figure 7). With the significant values being important and the small values appearing frequently, neither of them are negligible and need to be carefully quantized at the same time. Unfortunately, typical quantization methods fall short of this ability under low-bit settings, where the rounding error often outweighs the clipping error during optimization and results in over-clipped significant values, generating corrupted images. This inspires us to reshape the activation distributions via model finetuning to attain more quantization-friendly distributions, as depicted in Figure 1(a).

Property 2: Accurate temporal information is critical for quantization performance.

Diffusion model predictions are highly correlated with time step information. Specifically, time steps are transformed and projected into time embeddings and then added onto the image features, guiding the model to denoise correctly. Table 2 shows the performance comparison of quantizing time embeddings or preserving their full-precision values in the LDM-4 of LSUN-Bedrooms [39]. Under W8A8 and W4A8, quantizing the time embeddings leads to an increase of 0.81 and 1.04 (relatively 15%) in FID, respectively. This indicates that inaccurate time embedding quantization can lead to large degradation in generation performance, yielding even larger corruptions under lower bit-widths. Due to the different focus diffusion models have on image generation at different time steps, we infer that inaccurate time embeddings can cause mismatched input image and model functionality, resulting in possible oscillations in the sequence of noise removal. Thus, preserving diffusion model performance under quantization requires accurate temporal information.

Property 3: Different activations have different sensitivity towards decreasing bit-width.

Low-bit activation quantization is often more difficult than weight quantization and remains the key challenge for diffusion model quantization. Compared with weights that can be categorized into linear layers and convolutional layers, activation types are more diverse and complicated. Figure 3 shows the sensitivity of different layers’ activations to quantization. Specifically, we quantize three different types of activations to lower bits while maintaining the others’ bit-width to 8-bit, and observe how the decreasing bit-width effects generation performance. Surprisingly, we observe that the FeedForward layer [8] activations cause generation failure at as large as 6 bits, whereas the activations of all other linear layers (containing 5 times more layers) barely fail at 4 bits and all convolution layers (containing 3 times more layers) only fail at 4 bits. This indicates that a small amount of activations are especially sensitive to low-bit quantization, making them essential to be specially dealt with.

2.3 Quantization via Efficient Selective Finetuning

We first theoretically discuss the potential reasons for the failure of previous methods and the underlying rationale for weight fine-tuning. Then we introduce a finetuning method QuEST for

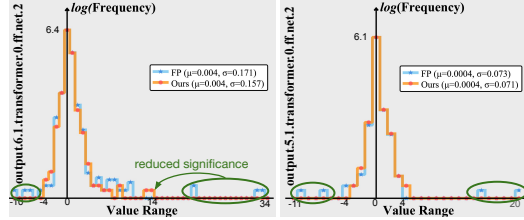


Figure 2: Illustration of imbalanced activation distributions. In the activation distribution of the full-precision model, the majority of values cluster near zero with sporadic large values, presenting challenges for low-bit quantization. Our method reduces the significant values to enable easier quantization for improved performance.

Table 2: Time embedding type comparison.

Bit-width	Time Embedding	FID ↓	sFID ↓
W8A8	PTQ Quantized	7.58	22.07
	Full Precision	6.77	22.03
	Ours	5.61	21.22
W4A8	PTQ Quantized	8.59	22.74
	Full Precision	7.55	21.69
	Ours	6.95	23.17

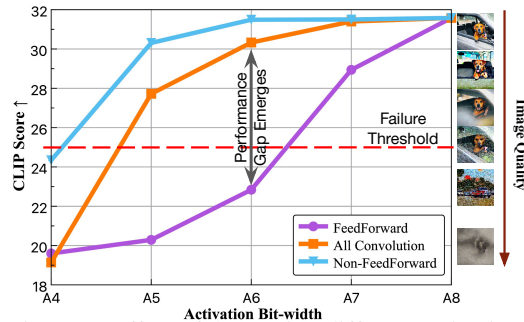


Figure 3: Effect of decreasing different activations’ bit-width on the model performance. The generation failure of FeedForward layers emerges at 6 bits, while all other linear layers barely fail at 4 bits and all convolution layers only fail at 4 bits.

diffusion models that can significantly boost low-bit performance with less time and memory usage. Figure 1(c) shows our framework, being a distillation-based finetuning strategy consisting of selective weight optimization and network-wise scaling factor optimization. To further address the loss of temporal information due to quantization, an efficient time-aware activation quantizer is proposed.

2.3.1 Sufficiency of Finetuning

Motivated by the phenomenon that current PTQ methods completely fail when applied to low-bit diffusion models and driven by the phenomenon that the performance degradation caused by activation bit-width decrease is much more significant than weight bit-width (8-bit to 4-bit) in diffusion models, we would like to explore theoretically why previous PTQ methods fail and how to overcome this.

We first review the underlying theory underpinning previous methods, which typically employ the reconstruction-based post-training quantization approach. Denote the diffusion model’s activations at time t as $\mathbf{z}_t = [z_{1,t}, z_{2,t}, \dots, z_{n,t}]$, the task loss as $L(z_{n,t}, \bar{z}_{n,t})$, where n is the number of layers and $\bar{z}_{n,t}$ is the ground-truth. L can be any loss function and here we use the mean squared error (MSE). We treat quantization as a type of perturbation and formulate the influence of activation quantization using Taylor expansion, assuming model weight \mathbf{w} is frozen:

$$\mathbb{E}[L(z_{n,t} + \Delta; \mathbf{w})] - \mathbb{E}[L(z_{n,t}; \mathbf{w})] \approx \Delta^T \bar{\mathbf{g}}^{(z_{n,t})} + \frac{1}{2} \Delta^T \bar{\mathbf{H}}^{(z_{n,t})} \Delta, \quad (3)$$

where Δ is the activation perturbation, $\bar{\mathbf{g}}^{(z)}$ is the gradient and $\bar{\mathbf{H}}^{(z_{n,t})}$ is the Hessian matrix. According to [22, 40], for a well-trained model, $\bar{\mathbf{g}}^{(z_{n,t})} = \nabla_{z_{n,t}} L$ approaches 0. Thus the above equation can be simplified to:

$$\frac{1}{2} \Delta^T \bar{\mathbf{H}}^{(z_{n,t})} \Delta = \frac{1}{2} (\tilde{z}_{n,t} - z_{n,t})^T \bar{\mathbf{H}}^{(z_{n,t})} (\tilde{z}_{n,t} - z_{n,t}). \quad (4)$$

This leads to a rather straightforward conclusion: Quantization error can be reduced by reconstructing the model output. However, under low-bit settings, the reasoning from Equation 3 to Equation 4 is inaccurate, where the activation perturbation Δ is too large for meaningful Taylor expansion. Thus we have the following proposition:

Proposition 2.1. *Reconstruction-based post-training quantization methods may lose their theoretical guarantee due to the large value perturbations under low-bit quantization.*

To resolve the above problem, we can use the following theorem by transforming Δ into a smaller perturbation ϵ :

Theorem 2.2. *Given an n layer diffusion model at time t with quantized activations as $\tilde{\mathbf{z}}_t = [\tilde{z}_{1,t}, \tilde{z}_{2,t}, \dots, \tilde{z}_{n,t}]$ and $\tilde{z}_{n,t} = z_{n,t} + \Delta$, where $z_{n,t}$ is the ground-truth and Δ is the large perturbation caused by low-bit quantization. Denote the target task MSE loss as $L(\tilde{z}_{n,t}, \bar{z}_{n,t})$, the quantization error can be transformed into:*

$$\begin{aligned} & \mathbb{E}[L(z_{n,t} + \Delta; \mathbf{w})] - \mathbb{E}[L(z_{n,t}; \mathbf{w})] \\ & \approx 2\epsilon^T \sum_{i=1}^K (\tilde{z}_{n-1,t}^i \cdot \mathbf{w}_n - z_{FP}) + \frac{1}{2} \sum_{i=1}^K (\tilde{z}_{n,t}^i - z_{FP})^T \bar{\mathbf{H}}^{(z_{n,t} + (i-1)\epsilon)} (\tilde{z}_{n,t}^i - z_{FP}) \end{aligned} \quad (5)$$

where \mathbf{w}_n is the weight for layer n and $\tilde{z}_{n,t}^i = \tilde{z}_{n-1,t}^i \cdot \mathbf{w}_n$, ϵ is a perturbation small enough for Taylor expansion, K is a constant and $\Delta = K\epsilon$.

Proof is provided in Appendix B. Theorem 2.2 indicates that: To minimize the quantization error, ideally we can finetune \mathbf{w}_n so that for any i , the weights can fit to the data/activation $\tilde{z}_{n-1,t}^i + (i-1)\epsilon$ which the full-precision counterpart may not fit, making the model more robust to varying inputs. In other words, **we are finetuning the model weights for better robustness towards large input activation perturbations, therefore enabling easier quantization.** We also find that the second term in Equation 5 can be minimized simultaneously with the first term, so that the total quantization error can be reduced via a common goal: Activation output alignment via finetuning \mathbf{w}_n .

2.3.2 Quantization via Selective Finetuning

Motivated by the unraveled properties of quantized diffusion models and the shortcomings in existing quantization approaches, we propose an efficient finetuning strategy for low-bit diffusion model quantization. The components of our method are detailed below.

Table 3: Unconditional image generation results of LDM-4 models on LSUN-Bedrooms/Churches 256×256. "N/A" denotes generation failure. "FP" denotes the full precision model.

Dataset	Method	Bit-width (W/A)	Size (MB)	FID↓	Dataset	Method	Bit-width (W/A)	Size (MB)	FID↓
LSUN-Bedrooms (LDM-4)	FP	32/32	1045.6	2.95	LSUN-Churches (LDM-8)	FP	32/32	1125.4	4.02
	PTQ4DM	8/8	279.1	4.75		PTQ4DM	8/8	330.6	5.54
	Q-Diffusion	8/8	279.1	4.53		Q-Diffusion	8/8	330.6	6.94
	PTQ-D	8/8	279.1	3.75		PTQ-D	8/8	330.6	6.40
	EfficientDM	8/8	279.1	2.98		EfficientDM	8/8	330.6	4.01
	Ours	8/8	279.1	3.07		Ours	8/8	330.6	6.55
	PTQ4DM	4/8	148.4	-		PTQ4DM	4/8	189.9	-
	Q-Diffusion	4/8	148.4	5.37		Q-Diffusion	4/8	189.9	7.80
	PTQ-D	4/8	148.4	5.94		PTQ-D	4/8	189.9	7.33
	EfficientDM	4/8	148.4	-		EfficientDM	4/8	148.4	-
Ours	4/8	148.4	3.26	Ours	4/8	189.9	7.33		
PTQ4DM	4/4	148.4	N/A	PTQ4DM	4/4	189.9	N/A		
Q-Diffusion	4/4	148.4	N/A	Q-Diffusion	4/4	189.9	N/A		
PTQ-D	4/4	148.4	N/A	PTQ-D	4/4	189.9	N/A		
EfficientDM	4/4	148.4	10.60	EfficientDM	4/4	148.4	14.34		
Ours	4/4	148.4	5.64	Ours	4/4	189.9	11.76		

Data-Free Partial-network-wise Training. To alleviate the need of substantial training data, we construct the calibration set in a data-free manner. By feeding sampled Gaussian noises x_T into the full-precision model and sample iteratively over different time steps, we can obtain the calibration data needed for finetuning the quantized model. In practice, the number of samples generated for each time step is 128 or 256, indicating that we only have to inference the full-precision model a few times to obtain the needed number of calibration samples.

As depicted in Figure 1(c), to overcome the quantization difficulty demonstrated in property ❶ efficiently, we update partial model weights (\mathbf{W}_{TE} and \mathbf{W}_A) that only account for a small subset of parameters related to the time step t . The other weight parameters (such as $\mathbf{W}_{I'}$, $\mathbf{W}_{I''}$) are frozen during optimization. For example on LDM-4 [32], at most 7% of the parameters are included for adjustment. The choices for the weights to be finetuned are discussed in the following sections. To better conserve the performance and behavior of the full-precision model, we use both its intermediate activations and final outputs as the ground-truth for supervision. Figure 4 visualizes the generation results and demonstrates the effectiveness of this strategy in preserving image details.

The activation quantization parameters can be viewed as additional model parameters, therefore we further propose a network-wise training strategy. Different from quantization methods using layer-wise or block-wise reconstruction [19, 34] that binds quantization parameters with their corresponding layers or blocks, we optimize all activation scaling factors for each time step together with the partial weight parameters. Additionally, while layer/block-wise optimization methods can only reconstruct sequentially, we update the required parameters at once. In this way, we significantly save the time and memory needed for quantization. Note that the quantization parameters for the weights are not updated once initialized, in order to maintain memory efficiency during deployment.

Efficient Time-aware Activation Quantization. As discussed in property ❷, accurate time embedding quantization is critical. To discriminate between different time steps, we design a temporal quantizer specifically for activation quantization that adopts different sets of quantization parameters for different time steps. While these parameters consumes negligible memory and does not effect inference speed, learning independent parameters for each time step leads to immense time cost.

Motivated by the fact that neighboring time steps yield similar functions in diffusion models [3], we cluster neighboring time steps so that they share the same quantization parameters and are calculated by the same calibration data x_t : $s(t) = s(t+1) = \dots = s(t+\Delta t)$, where the time steps used for optimization are sampled uniformly, and each chosen time step's statistics are used to represent Δt adjacent ones. Though most time steps' quantization parameters are approximated, this strategy saves the optimization time by t times without compromising much performance. Section 3.2 further provides an analysis on the performance and efficiency trade-off.

Selective & Progressive Layer Alignment. As investigated in Section 2.2, we identify two crucial types of activations for image generation performance and select them for weight finetuning: Time embeddings and attention-related activations (e.g. FeedForward layers in Stable Diffusion). We progressively update these components due to their distinct, non-overlapping functionalities.



Figure 4: Generated images compared with Q-Diffusion under two bit-width types: W8A8 and W4A4, using LDM-4 for LSUN-Bedrooms. Our method not only succeed well in generating low-bit images, but also aligns more closely with the full-precision counterpart.

In a single forward process, identical time embeddings are injected into different parts of the model, passed through projection layers, and merged with the latent image representations. This implies that the time information operates independently from the primary network flow. Thus, we first refine the time embedding layer l 's weight \mathbf{w}_l along with its activation quantization parameters $\mathbf{s}_l(t)$:

$$\mathcal{L}_{\text{TE}}^t = \sum_{l \in \mathbb{C}_{\text{TE}}} \mathbb{E}_t [\|\bar{O}(e(t); \mathbf{w}_l) - \tilde{O}(e(t); \mathbf{w}_l, \mathbf{s}_l(t))\|^2], \quad (6)$$

where \mathbb{C}_{TE} represents the set of time embedding layers, $e(t)$ is the fixed time embedding for time t . $\bar{O}(e(t); \mathbf{w}_l)$ is the final activation output of the full-precision model representing the ground-truth, and $\tilde{O}(e(t); \mathbf{w}_l, \mathbf{s}_l(t))$ is the quantized output. This objective function indicates that the chosen weight parameters are consistently updated across different time steps, so as to ensure robustness to diverse temporal inputs. Nevertheless, only the small subset of scaling factors relevant to each specific time step are adjusted for temporal information discrimination.

Apart from time embedding layers, attention-related layers are also vital (according to property ③). As depicted in Figure 3, reducing the activation bit-width of these layers degrades model performance the most dramatically. Denote \mathbb{C}_A as the set containing all these layers and given the image calibration samples x_t , we optimize the corresponding weights \mathbf{w}_l and quantization parameters $\mathbf{s}(t)$. However, we exclude the quantization parameters already optimized in Equation 6:

$$\mathcal{L}_A^t = \sum_{l \in \mathbb{C}_A} \mathbb{E}_t [\|\bar{O}(x_t; \mathbf{w}_{:l}) - \tilde{O}(x_t; \mathbf{w}_{:l}, \mathbf{s}(t) \setminus \mathbf{s}_{\mathbb{C}_{\text{TE}}}^t)\|^2], \quad (7)$$

where $\mathbf{w}_{:l}$ are the weight parameters of the first l layers. This strategy resembles linear probing, where only the layer directly associated with the activation output is finetuned.

Furthermore, we aim not only for each independent layer's quantization error reduction, but also for the final generated images' quality improvement. Therefore, we adopt the **Task Loss Guidance** strategy where the target task loss $\sum_t \mathcal{L}_d^t$ is introduced and the ground-truth is approximated by the output of the full-precision counterpart. By integrating Equation 6 and Equation 7, the final objective is formulated as follows:

$$\begin{aligned} \mathcal{L} &= \sum_t ((\mathcal{L}_{\text{TE}}^t + \mathcal{L}_d^t) + (\mathcal{L}_A^t + \mathcal{L}_d^t)) \\ &= \sum_t (\mathcal{L}_{\text{TE}}^t + \mathcal{L}_A^t + 2\mathbb{E}[\|\bar{O}(x_t; \mathbf{w}) - \tilde{O}(x_t; \mathbf{w}, \mathbf{s}(t))\|^2]). \end{aligned} \quad (8)$$

3 Experiments

3.1 Experiment Settings

To verify the effectiveness of our proposed method, we conduct experiments on three types of generation tasks: Unconditional image generation on LSUN-Bedrooms and LSUN-Churches datasets [39], class-conditional image generation on ImageNet [5], and text-to-image generation. The model architectures we quantize include LDM and Stable Diffusion [32], and uses "WnAm" to represent the quantization setting: n-bit weight quantization and m-bit activation quantization. DDIM samplers [15] are adopted for LDMs and the PLMS sampler [26] is used for Stable Diffusion. We generate 256 samples per time step for constructing the calibration set, and train 20 epochs over each time step. The Adam optimizer [18] is adopted and the learning rate for weight finetuning and scaling factor finetuning are set as $1e^{-5}$ and $1e^{-4}$ respectively.

We compare with popular Post-training Quantization methods including PTQ4DM [34], Q-Diffusion [19] and PTQ-D [12], as well as the state-of-the-art efficient finetuning method EfficientDM [11]. The performance of different quantized LDMs are evaluated using the Fréchet Inception Distance (FID) [14], spatial FID (sFID) [29] and Inception Score (IS) [1]. Unless specified, quantitative results are obtained by sampling 50,000 images and evaluated using the official evaluation scripts [6]. For Stable Diffusion, we use the CLIP Score [13] for evaluation. All experiments are conducted on A6000 GPUs using the PyTorch framework [30].

Table 4: Class-conditional generation results using LDM-4 on ImageNet 256×256.

Bit-width (W/A)	Method	Size (MB)	FID↓	sFID↓	IS↑
32/32	FP	1529.7	11.28	7.70	364.73
8/8	Q-Diffusion	428.7	10.60	9.29	350.93
	PTQ-D	428.7	10.05	9.01	359.78
	EfficientDM	435.0	11.38	8.04	362.34
	Ours	428.7	10.43	6.07	365.12
4/8	Q-Diffusion	237.5	9.29	9.29	336.80
	PTQ-D	237.5	8.74	7.98	344.72
	EfficientDM	243.8	9.93	7.34	353.83
	Ours	237.5	8.48	6.55	346.02
4/4	Q-Diffusion	237.5	N/A	N/A	N/A
	PTQ-D	237.5	N/A	N/A	N/A
	EfficientDM	243.8	6.17	7.75	250.90
	Ours	237.5	5.98	7.93	202.45

3.2 Experiment Results and Analysis

Unconditional Generation: We evaluate the performance of our method over LDM-4 (LSUN-Bedrooms 256×256) and LDM-8 (LSUN-Churches 256×256) using the DDIM sampler with 200 and 500 time steps, respectively. Results are shown in table 3. The results are evaluated using FID, where the Inception Score is not a reasonable metric for datasets that have significantly different domains and categories from ImageNet [19].

Class-conditional Generation: We evaluate the performance using LDM-4 on ImageNet 256×256 using the DDIM sampler (20 steps). As shown in Table 4, three metrics are used for evaluation. Note that sFID uses additional intermediate spatial features for calculation compared with FID. We can also see that FID is not a valid metric for ImageNet LDM-4 evaluation: All methods have lower FID when quantized to lower-bits, conflicting with human perception. We show that our method not only succeeds in W4A4 quantization, but also significantly improve the generation quality on higher bit settings. Under W8A8, our method is able to achieve 2.82 improvement over sFID and 8.13 increase in Inception Score. Under W4A8, we improve the SOTA PTQ method by 1.57 sFID and 8.77 IS.

Text-to-image Generation: We use Stable Diffusion v1.4 as the model for quantization with the PLMS sampler sampling 50 time steps. Table 5 shows the results. Images are generated based on the 10,000 prompts sampled from the COCO2014 [24] validation set, and CLIP Score is calculated based on the ViT-B/16 backbone. Given the limited works done on Stable Diffusion, we can only compare with Q-Diffusion and the full-precision baseline.

Efficiency comparison and effects of components. Table 6 compares with and without the use of task loss \mathcal{L}_d . The results show that using the difference between the outputs of the quantized model and the full-precision counterpart for supervision is essential for performance improvement, enhancing the FID by 2.58 and 5.21 for SLA_{TE} and SLA_A , respectively. However, when the learning process is only supervised by the task loss, the performance degrades by 7.13 FID and 9.39 sFID for SLA_{TE} , indicating that the task loss alone is insufficient.

Table 5: Text-to-image generation on Stable Diffusion (512×512) using COCO2014 prompts.

Bit-width (W/A)	Method	Size (MB)	CLIP Score↑
32/32	FP	3279.1	31.50
8/8	Q-Diffusion	949.0	31.43
	Ours	949.0	31.47
4/8	Q-Diffusion	539.1	31.39
	Ours	539.1	31.50
4/4	Q-Diffusion	539.1	N/A
	Ours	539.1	28.85

Table 6: Influence of task loss supervision on model performance.

Method	SLA_{TE}	SLA_{TE}	SLA_A	SLA_A
	w/o \mathcal{L}_d	w/ \mathcal{L}_d	w/o \mathcal{L}_d	w/ \mathcal{L}_d
FID↓	8.99	6.41	11.41	6.20
sFID↓	15.23	11.18	15.64	12.32

Table 7: Component and efficiency comparisons on LDM-4 (LSUN-Bedrooms 256×256).

Method	Bit-width (W/A)	Calibration data size	Time cost (GPU hours)	Memory cost (MB)	Model size (MB)	FID↓
FP	32/32	-	-	-	1045.6	2.95
PTQ [19]	4/8	5120	23.08	10334	148.4	5.37
Baseline	4/8	5120	11.52	9822	148.4	6.95
+ SLA _A	4/8	5120	13.13	12134	148.4	4.41
+ SLA _A + SLA _{TE}	4/8	5120	15.25	12450	148.4	3.26

Table 7 compares efficiency and performance between our method and the post-training quantization approach on the LSUN-Bedrooms dataset when using LDM-4. Our approach, while utilizing the same quantity of calibration data as the PTQ method, is more time-efficient and incurs only a 20% increase in GPU memory usage. We also show how each proposed component improves the generation performance. The results indicate that sequentially finetuning time embedding layers followed by finetuning attention-related layers leads to consistent performance improvements.

Time step sampling frequency analysis. While time steps are sampled uniformly, will the performance consistently improve when we sample more frequently? Figure 5 illustrates the trade-off between the increased number of sampled time steps ('T-Num') and generation performance. Metrics are calculated using 10,000 samples generated from LDM-4 on LSUN-Bedrooms. The results show that though performance improves consistently, the amount of growth gradually decreases. Starting from 5 time steps, using 15 more time steps leads to 25.22 sFID improvement. But using another 30 time steps (from 20 to 50) only leads to 2.92 sFID improvement. Given the linearly increasing time cost associated with using more time steps, we opt for only 20 out of 200 time steps to enhance quantization efficiency.

How QuEST influences model properties. Our approach is based on the certain characteristics observed in quantized diffusion models, hence we aim to analyze how our fine-tuning strategy counters these identified challenges. As shown in Table 2, finetuning time embedding layers leads to even better performance than the full-precision counterpart. We infer that this might be due to both the additional parameters introduced by quantization and the additional task loss supervision. Figure 2 further implies that our method adjusts the activation distribution so that it can be more easily quantized. We see that the ranges of the activation value distributions shrink from [-10, 34] to [-4, 14] and [-11, 20] to [-4, 4]. The standard deviations also decrease from 0.171 to 0.157 and from 0.073 to 0.071. This indicates a higher concentration of values around the mean, which can effectively reduce both rounding and clipping errors.

Integration with LoRA finetuning. Finetuning quantized models is not trivial. Thus, we use QALoRA [11] that extends LoRA [16] and finetune on the ImageNet 256×256 dataset. The weight rank of 32 is used for the LoRA modules and the parameters are trained over 100 time steps for 160 epochs. We find that integrating the QALoRA technique leads to a 5.62 decrease in FID, indicating that finetuning the original layers is a better solution for performance preservation.

4 Conclusion

We have proposed QuEST, an efficient data-free finetuning framework for low-bit diffusion model quantization. Our method is motivated and guided by the three underlying properties found in quantized diffusion models. We also theoretically demonstrate the sufficiency of finetuning, interpreting it as a way to enhance model robustness against large activation perturbations. To alleviate the performance degradation, we propose to finetune the time embedding layers and the attention-related layers under the supervision of the full-precision counterpart. Experimental results on three high-resolution image generation tasks (including Stable Diffusion) demonstrate the effectiveness and efficiency of QuEST, achieving low-bit compatibility with less time and memory cost.

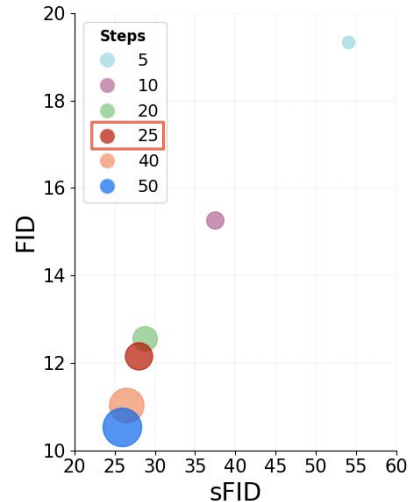


Figure 5: Effect of uniformly sampled time steps number. Circle size represents quantization computation cost. Red square indicates the value we choose.

References

- [1] Shane Barratt and Rishi Sharma. A note on the inception score, 2018.
- [2] Krishna Teja Chitty-Venkata, Sparsh Mittal, Murali Emani, Venkatram Vishwanath, and Arun K Somani. A survey of techniques for optimizing transformer inference. *Journal of Systems Architecture*, page 102990, 2023.
- [3] Jooyoung Choi, Jungbeom Lee, Chaehun Shin, Sungwon Kim, Hyunwoo Kim, and Sungroh Yoon. Perception prioritized training of diffusion models, 2022.
- [4] Florinel-Alin Croitoru, Vlad Hondru, Radu Tudor Ionescu, and Mubarak Shah. Diffusion models in vision: A survey. *IEEE Transactions on Pattern Analysis and Machine Intelligence*, 45(9):10850–10869, 2023.
- [5] Jia Deng, Wei Dong, Richard Socher, Li-Jia Li, Kai Li, and Li Fei-Fei. Imagenet: A large-scale hierarchical image database. In *2009 IEEE conference on computer vision and pattern recognition*, pages 248–255. IEEE, 2009.
- [6] Prafulla Dhariwal and Alex Nichol. Diffusion models beat gans on image synthesis, 2021.
- [7] Alexey Dosovitskiy, Lucas Beyer, Alexander Kolesnikov, Dirk Weissenborn, Xiaohua Zhai, Thomas Unterthiner, Mostafa Dehghani, Matthias Minderer, Georg Heigold, Sylvain Gelly, Jakob Uszkoreit, and Neil Houlsby. An image is worth 16x16 words: Transformers for image recognition at scale, 2021.
- [8] Zhida Feng, Zhenyu Zhang, Xintong Yu, Yewei Fang, Lanxin Li, Xuyi Chen, Yuxiang Lu, Jiayang Liu, Weichong Yin, Shikun Feng, Yu Sun, Li Chen, Hao Tian, Hua Wu, and Haifeng Wang. Ernie-vilg 2.0: Improving text-to-image diffusion model with knowledge-enhanced mixture-of-denoising-experts. In *Proceedings of the IEEE/CVF Conference on Computer Vision and Pattern Recognition (CVPR)*, pages 10135–10145, June 2023.
- [9] Amir Gholami, Sehoon Kim, Zhen Dong, Zhewei Yao, Michael W Mahoney, and Kurt Keutzer. A survey of quantization methods for efficient neural network inference. In *Low-Power Computer Vision*, pages 291–326. Chapman and Hall/CRC, 2022.
- [10] Kaiming He, Xiangyu Zhang, Shaoqing Ren, and Jian Sun. Deep residual learning for image recognition, 2015.
- [11] Yefei He, Jing Liu, Weijia Wu, Hong Zhou, and Bohan Zhuang. Efficientdm: Efficient quantization-aware fine-tuning of low-bit diffusion models, 2023.
- [12] Yefei He, Luping Liu, Jing Liu, Weijia Wu, Hong Zhou, and Bohan Zhuang. Ptqd: Accurate post-training quantization for diffusion models, 2023.
- [13] Jack Hessel, Ari Holtzman, Maxwell Forbes, Ronan Le Bras, and Yejin Choi. Clipscore: A reference-free evaluation metric for image captioning, 2022.
- [14] Martin Heusel, Hubert Ramsauer, Thomas Unterthiner, Bernhard Nessler, and Sepp Hochreiter. Gans trained by a two time-scale update rule converge to a local nash equilibrium, 2018.
- [15] Jonathan Ho, Ajay Jain, and Pieter Abbeel. Denoising diffusion probabilistic models, 2020.
- [16] Edward J. Hu, Yelong Shen, Phillip Wallis, Zeyuan Allen-Zhu, Yuanzhi Li, Shean Wang, Lu Wang, and Weizhu Chen. Lora: Low-rank adaptation of large language models, 2021.
- [17] Benoit Jacob, Skirmantas Kligys, Bo Chen, Menglong Zhu, Matthew Tang, Andrew Howard, Hartwig Adam, and Dmitry Kalenichenko. Quantization and training of neural networks for efficient integer-arithmetic-only inference, 2017.
- [18] Diederik P. Kingma and Jimmy Ba. Adam: A method for stochastic optimization, 2017.
- [19] Xiuyu Li, Yijiang Liu, Long Lian, Huanrui Yang, Zhen Dong, Daniel Kang, Shanghang Zhang, and Kurt Keutzer. Q-diffusion: Quantizing diffusion models. In *Proceedings of the IEEE/CVF International Conference on Computer Vision (ICCV)*, pages 17535–17545, October 2023.
- [20] Yanjing Li, Sheng Xu, Xianbin Cao, Baochang Zhang, and Xiao Sun. Q-dm: An efficient low-bit quantized diffusion model. In *NeurIPS 2023*, October 2023.
- [21] Yanjing Li, Sheng Xu, Baochang Zhang, Xianbin Cao, Peng Gao, and Guodong Guo. Q-vit: Accurate and fully quantized low-bit vision transformer, 2022.

- [22] Yuhang Li, Ruihao Gong, Xu Tan, Yang Yang, Peng Hu, Qi Zhang, Fengwei Yu, Wei Wang, and Shi Gu. Brecq: Pushing the limit of post-training quantization by block reconstruction. *arXiv preprint arXiv:2102.05426*, 2021.
- [23] Tailin Liang, John Glossner, Lei Wang, Shaobo Shi, and Xiaotong Zhang. Pruning and quantization for deep neural network acceleration: A survey. *Neurocomputing*, 461:370–403, 2021.
- [24] Tsung-Yi Lin, Michael Maire, Serge Belongie, Lubomir Bourdev, Ross Girshick, James Hays, Pietro Perona, Deva Ramanan, C. Lawrence Zitnick, and Piotr Dollár. Microsoft coco: Common objects in context, 2015.
- [25] Jiawei Liu, Lin Niu, Zhihang Yuan, Dawei Yang, Xinggang Wang, and Wenyu Liu. Pd-quant: Post-training quantization based on prediction difference metric, 2023.
- [26] Luping Liu, Yi Ren, Zhijie Lin, and Zhou Zhao. Pseudo numerical methods for diffusion models on manifolds, 2022.
- [27] Markus Nagel, Rana Ali Amjad, Mart Van Baalen, Christos Louizos, and Tijmen Blankevoort. Up or down? adaptive rounding for post-training quantization. In *International Conference on Machine Learning*, pages 7197–7206. PMLR, 2020.
- [28] Yury Nahshan, Brian Chmiel, Chaim Baskin, Evgenii Zheltonozhskii, Ron Banner, Alex M Bronstein, and Avi Mendelson. Loss aware post-training quantization. *Machine Learning*, 110(11-12):3245–3262, 2021.
- [29] Charlie Nash, Jacob Menick, Sander Dieleman, and Peter W. Battaglia. Generating images with sparse representations, 2021.
- [30] Adam Paszke, Sam Gross, Francisco Massa, Adam Lerer, James Bradbury, Gregory Chanan, Trevor Killeen, Zeming Lin, Natalia Gimelshein, Luca Antiga, Alban Desmaison, Andreas Köpf, Edward Yang, Zach DeVito, Martin Raison, Alykhan Tejani, Sasank Chilamkurthy, Benoit Steiner, Lu Fang, Junjie Bai, and Soumith Chintala. Pytorch: An imperative style, high-performance deep learning library, 2019.
- [31] Ratko Pilipović, Patricio Bulić, and Vladimir Risojević. Compression of convolutional neural networks: A short survey. In *2018 17th International Symposium INFOTEH-JAHORINA (INFOTEH)*, pages 1–6. IEEE, 2018.
- [32] Robin Rombach, Andreas Blattmann, Dominik Lorenz, Patrick Esser, and Björn Ommer. High-resolution image synthesis with latent diffusion models, 2021.
- [33] Olaf Ronneberger, Philipp Fischer, and Thomas Brox. U-net: Convolutional networks for biomedical image segmentation, 2015.
- [34] Yuzhang Shang, Zhihang Yuan, Bin Xie, Bingzhe Wu, and Yan Yan. Post-training quantization on diffusion models. In *CVPR*, 2023.
- [35] Changyuan Wang, Ziwei Wang, Xiuwei Xu, Yansong Tang, Jie Zhou, and Jiwen Lu. Towards accurate data-free quantization for diffusion models, 2023.
- [36] Peisong Wang, Qiang Chen, Xiangyu He, and Jian Cheng. Towards accurate post-training network quantization via bit-split and stitching. In *International Conference on Machine Learning*, pages 9847–9856. PMLR, 2020.
- [37] Xiuying Wei, Ruihao Gong, Yuhang Li, Xianglong Liu, and Fengwei Yu. Qdrop: Randomly dropping quantization for extremely low-bit post-training quantization, 2023.
- [38] Sheng Xu, Yanjing Li, Mingbao Lin, Peng Gao, Guodong Guo, Jinhu Lu, and Baochang Zhang. Q-detr: An efficient low-bit quantized detection transformer, 2023.
- [39] Fisher Yu, Yinda Zhang, Shuran Song, Ari Seff, and Jianxiong Xiao. Lsun: Construction of a large-scale image dataset using deep learning with humans in the loop. *arXiv preprint arXiv:1506.03365*, 2015.
- [40] Zhihang Yuan, Chenhao Xue, Yiqi Chen, Qiang Wu, and Guangyu Sun. Ptq4vit: Post-training quantization framework for vision transformers with twin uniform quantization, 2022.

A Related Works

A.1 Diffusion Model Inference

Diffusion models [15, 32] generate samples via a learned iterative denoising process. During inference, the initial input is sampled from a Gaussian distribution: $x_T \sim \mathcal{N}(\mathbf{0}, \mathbf{I})$, and the final output x_0 is obtained by removing noises from x_T subsequently using:

$$p_\theta(x_{t-1}|x_t) = \mathcal{N}(x_{t-1}; \tilde{\boldsymbol{\mu}}_{\theta,t}(x_t), \tilde{\boldsymbol{\beta}}_t \mathbf{I}). \quad (9)$$

In this Markov Chain, $\tilde{\boldsymbol{\mu}}_{\theta,t}$ and $\tilde{\boldsymbol{\beta}}_t$ are calculated from the model’s output. For a typical diffusion model, the denoising stage requires hundreds to thousands of iterations. This laborious sequential process makes efficient inference and high-resolution generation extremely challenging. Latent Diffusion Models (LDMs) [32] were developed to overcome the challenges. They encode the data into a latent space and then apply the diffusion process within this space, enabling high-resolution image generation with fewer time steps. The output images are produced by decoding the latent representations. LDM’s concept and network quantization complement each other, mutually enhancing the efficiency of diffusion models.

Practically, diffusion models typically adopt a UNet architecture [33], with some modules substituted by attention blocks. In a latent diffusion model, an encoder and a decoder are incorporated for projecting images into latent representations and subsequently generating images from the latent space, respectively. Usually encoders and decoders are lightweight and computationally inexpensive, so our focus is on quantizing the UNets in LDMs, in alignment with other works (as described below).

A.2 Diffusion Model Quantization

Model quantization is a dominant technique for optimizing the inference memory and speed of deep learning models by reducing the precision of the tensors used in computation. Few researches were done for quantizing diffusion models and they fall into two mainstream frameworks: Quantization-Aware Training (QAT) [17, 20, 21, 38] and Post-Training Quantization (PTQ) [22, 25, 28, 36, 37]. QAT methods such as Q-DM [20] consider value precision as an additional optimization constraint, training all parameters from scratch with the target task objective. While it is effective for low-bit quantization, it is even more resource-intensive than training a full-precision model. Efficient-DM [11] further uses Low-rank adapters (LoRA) [16] to reduce training cost. However, it introduces extra weight parameters and still requires substantial training iterations.

Post-Training Quantization methods aim to calibrate the quantization parameters based on a small calibration set. Pioneering works such as PTQ4DM [34] and Q-Diffusion [19] focus on sampling the outputs of the full-precision model under different time steps with certain probabilities to construct the calibration set. ADP-DM [35] partition time steps into different groups and optimize each group with differentiable search algorithms. PTQ-D [12] decomposes the quantization noise and correct them individually with full-precision model statistics. However, these methods generally fail under 4-bit or lower bit-width. To enable low-bit compatibility with high efficiency, our method adopts the general framework of PTQ but further introduces an efficient weight fine-tuning strategy.

B Proof for Theorem 2.2

We provide the detailed proof for Theorem 2.2 here. The notations are consistent with the ones in the main paper.

Since the perturbation Δ is too large for accurate Taylor expansion, we can resolve it by introducing a new perturbation $\epsilon = \Delta/K$, where we divide Δ by a constant K so that ϵ is small enough for

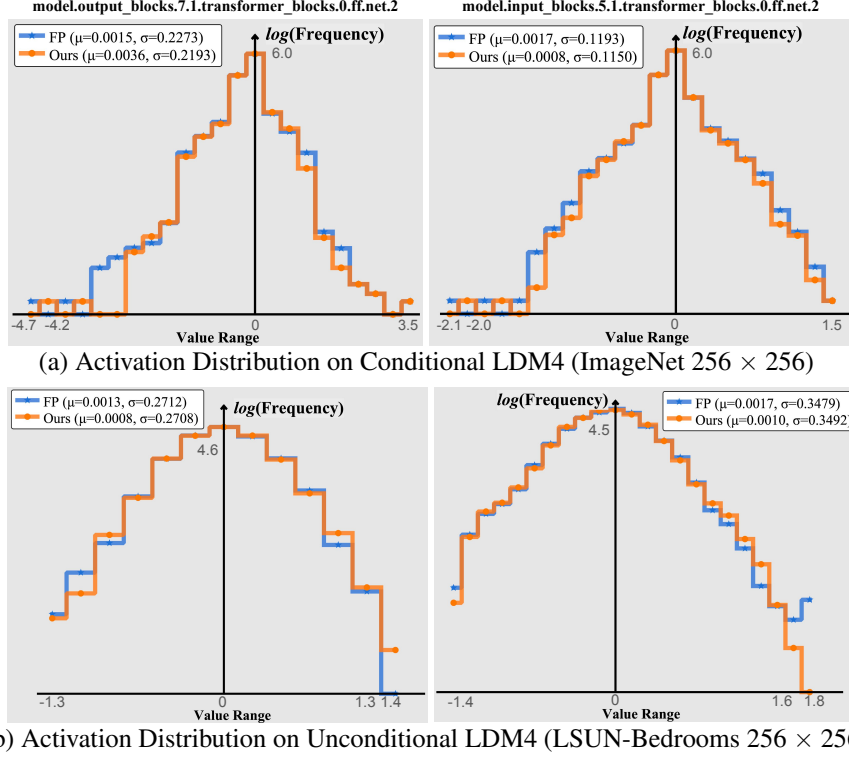


Figure 6: Illustrations of imbalanced activation distributions on conditional LDM4 (ImageNet 256×256) and unconditional LDM4 (LSUN-Bedrooms 256×256).

approximation. Then, Equation 3 is rewritten as follows:

$$\begin{aligned}
& \mathbb{E}[L(z_{n,t} + \Delta; \mathbf{w})] - \mathbb{E}[L(z_{n,t}; \mathbf{w})] \\
&= \sum_{i=1}^K \left(\mathbb{E}[L(z_{n,t} + \frac{i}{K}\Delta; \mathbf{w})] - \mathbb{E}[L(z_{n,t} + \frac{i-1}{K}\Delta; \mathbf{w})] \right) \\
&\approx \sum_{i=1}^K \left(\epsilon^T \bar{\mathbf{g}}^{(z_{n,t} + (i-1)\epsilon)} + \frac{1}{2} \epsilon^T \bar{\mathbf{H}}^{(z_{n,t} + (i-1)\epsilon)} \epsilon \right), \tag{10}
\end{aligned}$$

where the approximation step follows Taylor expansion and only the first two main components are kept. The first term in Equation 10 cannot be ignored because samples such as $z_{n,t} + (i-1)\epsilon$ may not be included in the learned distribution of the model. The second term can still be minimized by reconstruction since only the difference between quantized model output and ground-truth matters. In the following, we temporarily exclude the second term for simplicity since it can always be minimized through aligning the activation outputs.

Given the objective function (MSE loss) of diffusion models, we analyze that:

$$\begin{aligned}
\sum_{i=1}^K \epsilon^T \bar{\mathbf{g}}^{(z_{n,t} + (i-1)\epsilon)} &= 2\epsilon^T \sum_{i=1}^K (\tilde{z}_{n-1,t}^i \cdot \mathbf{w}_n - \bar{z}_{n,t}) \\
&\approx 2\epsilon^T \sum_{i=1}^K (\tilde{z}_{n-1,t}^i \cdot \mathbf{w}_n - z_{\text{FP}}), \tag{11}
\end{aligned}$$

where \mathbf{w}_n is the weight for layer n , $\tilde{z}_{n-1,t}^i$ is the activation of the $(n-1)$ th layer in a quantized model to get $z_{n,t} + (i-1)\epsilon$. Ground-truth $\bar{z}_{n,t}$ can be approximated by the full-precision output z_{FP} . We see that $\tilde{z}_{n-1,t}^i$ and z_{FP} cannot be changed, thus to minimize Equation 11, we need to finetune \mathbf{w}_n . From a general perspective, Equation 11 also indicates that the model has not converged well to a local minimum given the perturbed inputs, thus when we finetune the model layers given the

quantized inputs, we are actually training the model towards convergence over new samples and increasing its robustness.

C Examples of Imbalanced Activation Distributions

Apart from Figure 2, we show that the imbalance in the activation distribution is a common phenomenon in different model structures and datasets. In Figure 6, we show more results of activation distributions of latent diffusion models on ImageNet 256×256 and LSUN-Bedrooms 256×256 .

D Importance of large values in activations

As shown in Figure 2, quite a few values are rather large and diversely distributed. These values pose difficulties on activation quantization, and being rather important and not negligible. To demonstrate this, we corrupt certain tokens in the activation outputs of the diffusion model and check the corresponding generated images. The corruption is done by setting the token values as all zeros. As shown in Figure 7, we compare two settings: (1) corrupt a certain number of tokens randomly; (2) corrupt the same number of the tokens with the largest values.

We see that when corrupting randomly, generation performance is hardly effected. However, corrupting the same amount of tokens (even only one token) with the largest values leads to significantly degenerated images.

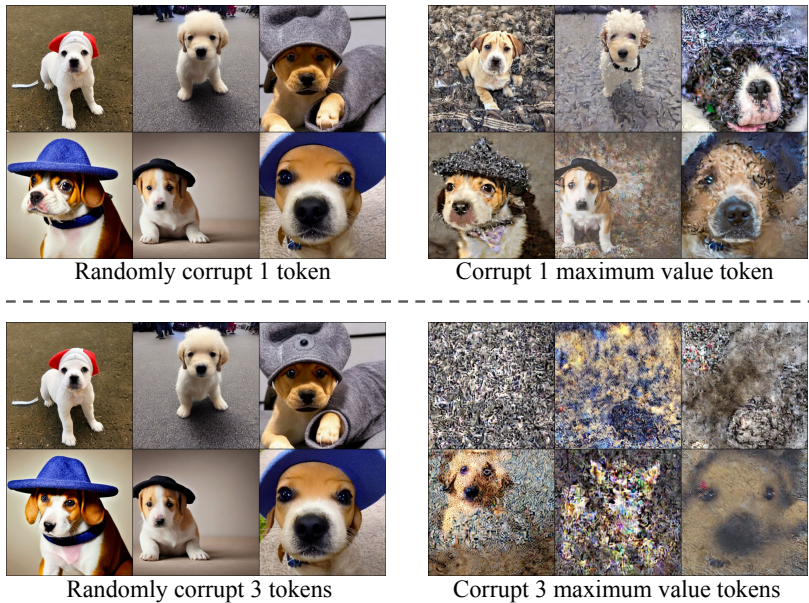


Figure 7: Comparison of different corruptions made on different tokens.

E Generated image examples for different tasks

E.1 Unconditional Image Generation

The generated images for LDM-4 on LSUN-Bedrooms 256×256 under different bit-widths are shown in Figure 8. Images for LSUN-Churches 256×256 are shown in Figure 9.

E.2 Class-conditional image generation

Figure 10 shows the generated images for 3 different classes.



Figure 8: Unconditional image generation examples for LSUN-Bedrooms 256×256 .

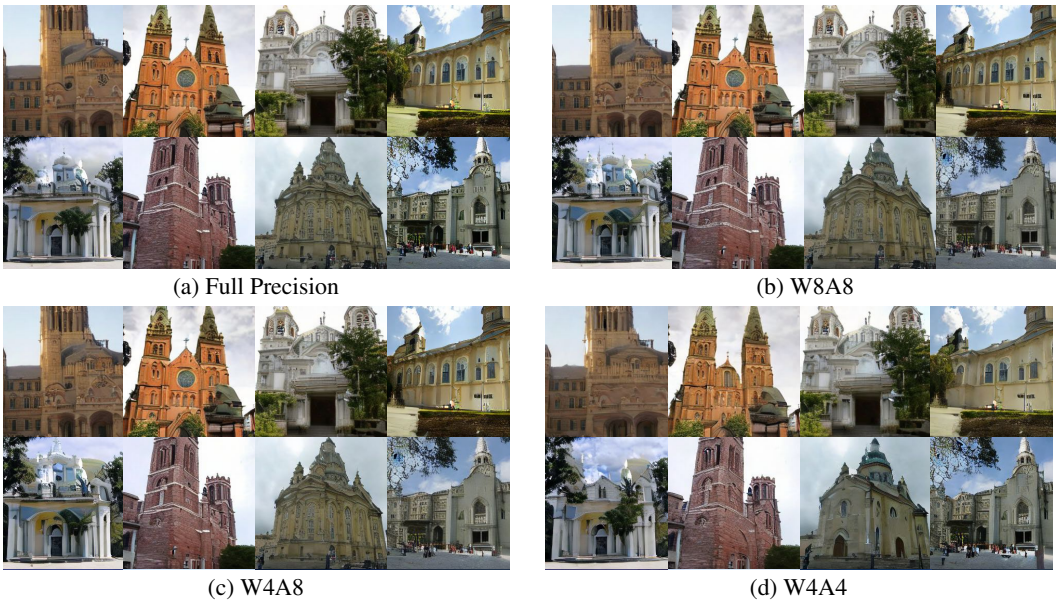


Figure 9: Unconditional image generation examples for LSUN-Churches 256×256 .

E.3 Text-to-image generation

Figure 11 shows the generated images for two different prompts using Stable Diffusion v1.4 under different bit-width.

F Limitations and Broader Impacts

The primary objective of this paper is to further the research in enhancing the efficiency of diffusion models. While it confronts societal consequences akin to those faced by research on generative models, it is important to recognize the potential impacts that quantized models could have on current techniques, including watermarking and safety checking. Inappropriate integration of current methodologies may result in unforeseen performance issues, a factor that deserves attention and awareness.

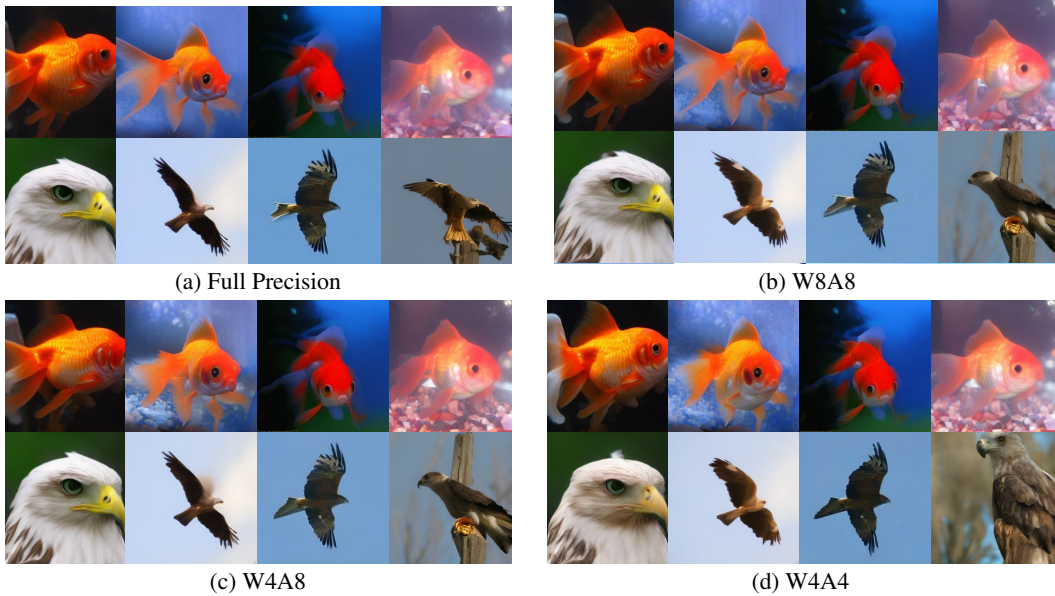


Figure 10: Conditional image generation results for ImageNet 256×256 .

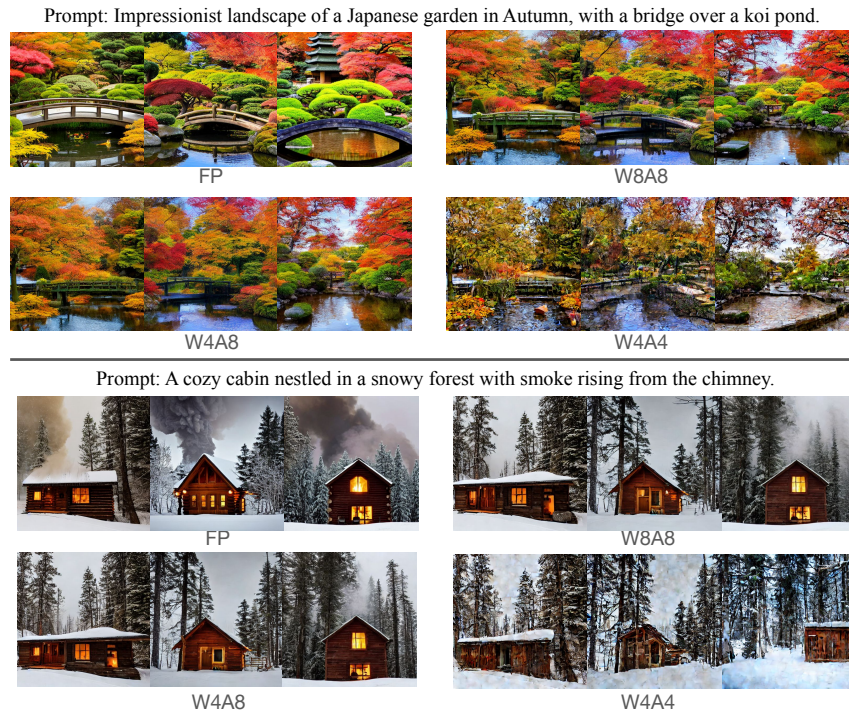


Figure 11: Text-to-image generation results on Stable Diffusion.